Basic network structure of SiO_2-B_2O_3-Na_2O glasses from diffraction and Reverse Monte Carlo simulation

M. Fábián[1,2*], Cs. Araczki[3]

[1]*Centre for Energy Research, H-1525 Budapest, P.O.B. 49, Hungary*
[2]*Wigner Research Centre for Physics, H-1525 Budapest, P.O.B. 49, Hungary*
[3]*Budapest University of Technology and Economics, Institute of Nuclear Techniques, Műegyetem rkp. 9, H-1111 Budapest, Hungary*
*Corresponding Author: fabian.margit@energia.mta.hu

Abstract

Neutron- and high-energy synchrotron X-ray diffraction experiments have been performed on the $(75-x)SiO_2$-xB_2O_3-$25Na_2O$ x=5, 10, 15 and 20 mol% glasses. The structure factor has been measured over a broad momentum transfer range, between 0.4-22 Å^{-1}. For data analyses and modeling the Fourier transformation and the RMC simulation techniques have been applied. The partial atomic pair correlation functions, the nearest neighbour distances, coordination number distributions and average coordination number values and three-particle bond angle distributions have been revealed. The Si-O network proved to be highly stable consisting of SiO_4 tetrahedral units with characteristic distances at r_{Si-O}=1.60 Å and r_{Si-Si}=3.0(5) Å. The behaviour of network forming boron atoms proved to be more complex. The first neighbour B-O distances show two distinct values at 1.30 Å and a characteristic peak at 1.5(5) Å and, both trigonal BO_3 and tetrahedral BO_4 units are present. The relative abundance of BO_4 and BO_3 units depend on the boron content, and with increasing boron content the number of BO_4 is decreasing, while BO_3 is increasing.

Keyword: borosilicate glasses, neutron and X-ray diffraction, RMC simulation

1. Introduction

Recently, several experiments have been reported on the study of structure and properties of sodium borosilicate glasses from fundamental and industrial point of view, due to the potential applicability for immobilizing of high-level radioactive wastes, like U-, Pu-, Th-oxides [1-7 and therein]. It has been found that the modifier effect of Na ions influences the ratio of nature of glass network formers Si, B and it is possible to archive a mixed glass network former effect. This effect is believed to have a structural origin, yet a precise understanding of it is still lacking because of the structural complexity of the sodium borosilicate glasses. The structure of borate glasses with alkali oxides has been extensively studied. A nuclear magnetic resonance (NMR) spectroscopy measurements show that the fraction of boron atoms tetrahedral coordinated to the total number of boron atoms varied with the modifier compositions [8-10]. By Raman spectroscopy, typical borate groups, such as boroxol, trigonal and tetrahedral units were found to exist in several borate compounds [11,12].

Recently, we have started to examined the atomic structure of a newly prepared three-component sodium-borosilicate system, using a combination of neutron diffraction (ND), high-energy X-ray diffraction (XRD) and reverse Monte Carlo (RMC) modelling that are capable of building three-dimensional structure models and so yield a more detailed description of the atomic-scale glass structure. In our previous works we studied the binary sodium silicate glasses $(70SiO_2$-$30Na_2O)$ [13], the binary sodium borate glasses $(75B_2O_3$-$25Na_2O)$ [14] and a five-component sodium borosilicate glass $(55SiO_2$-$25Na_2O$-$10B_2O_3$-$5BaO$-$5ZrO_2)$ [15]. Here, we apply the same approach to a ternary

system $(75-x)SiO_2-xB_2O_3-25Na_2O$ with x=5-20 mol%. We studied these simplified glasses containing only three main oxides which will be the main components - simultaneously changing the boron and sodium concentration - of our matrix-glasses doped with special actinides and lanthanides. The special interest of this system lies in the different glass forming mechanism of SiO_2 and B_2O_3. One of the main questions is the structural changes of the boron-oxygen network and the coordination around B atom induced by increasing B_2O_3 glass forming oxide. Nuclear Magnetic Resonance (NMR) spectroscopy was also applied to get complementary information on the boron environment.

2. Experimental details

2.1. Sample preparation

Samples in a glass phase were prepared with composition $(75-x)SiO_2-xB_2O_3-25Na_2O$, where x= 5, 10, 15, 20 mol% (hereafter referred as SiB5NaO, SiB10NaO, SiB15NaO and SiB20NaO, respectively) by conventional melt-quench technique using a high temperature electrical furnace with a platinum crucible under atmospheric conditions. The raw materials used were all of p.a. grade, SiO_2, Na_2O supplied by VWR International Co. and B_2O_3 by Sigma-Aldrich Co.. B_2O_3 was isotopically enriched in ^{11}B (99.6%, determined by Inductively Coupled Plasma Mass Spectroscopy technique [16]) in order to reduce the influence of the high neutron absorption of ^{10}B present in natural boron. The specimens were homogenized, and they are heated in a LAC high-temperature furnace at 1250°C for 40 min, and then melted in a range 1400-1450°C, for about 1.5h. The melt was stirred every half hour for proper mixing. The melt was cooled to 1250 °C pouring temperature, and kept there for 30 min. The melt was quickly poured on a stainless steel plate. The glasses thus obtained were found to be transparent. Powder samples were prepared by using an agate mortar. The samples proved to be fully amorphous, no visible inhomogeneities or crystalline phase was detected. For borosilicate glasses often it is a problem that the glass is hydrolytic, and with time it becomes humid. As far as ND and PGAA methods are sensitive experimental tools for hydrogen detection, we have regularly checked the amorphous and the hydrolytic state of the glasses. The glasses possess good chemical and hydrolytic stability. The elemental composition was verified by Prompt Gamma Activation Analysis [17, 18], the nominal and the measured values are the same within ~1%.

2.2. Nuclear Magnetic Resonance experiments and results

Nuclear Magnetic Resonance (NMR) experiments were recorded on the 600 MHz Varian NMR System equipped with the 3.2 MAS probe installed in the Slovenian NMR Centre in Ljubljana, Slovenia [19]. Spectra were acquired with single pulse sequence using non-selective 0.6 μs pulse and XiX decoupling during acquisition. Relaxation delay was 10 s and the sample rotation frequency was 20 kHz. 200 scans were accumulated during each measurement.

Figure 1 displays the measured ^{11}B NMR spectra. Two characteristic contributions have been detected: peak positioned around 0 ppm and a broader quadrupolar line between 5 and 20 ppm. Based on the literature ([20] and [21]) we assigned these two contributions to $^{[4]}B(BO_4)$ and $^{[3]}B(BO_3)$ structural units, as indicated in Figure 1. The peak intensities clearly show concentration dependence. The intensity of the $^{[3]}B$ peak increases with increasing boron content while the $^{[4]}B$ peak decreases. The maximum increase/decrease of the either peak's area was about 15% as determined by integration of the area under the two contributions. Detailed analysis of the NMR experiment is underway, and will be published elsewhere.
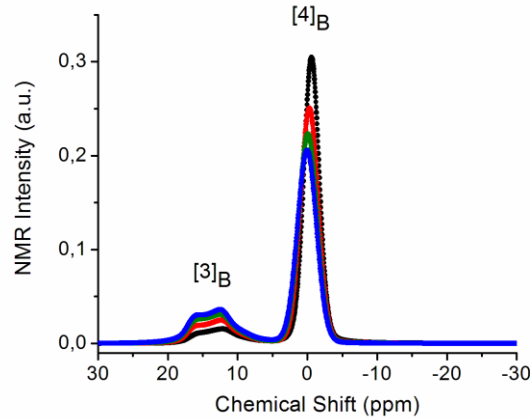
Figure 1. ^{11}B NMR spectra of glasses: SiB5NaO (black circle), SiB10NaO (red triangle), SiB15NaO (green square) and SiB20NaO (blue crosses).

2.3. Neutron and X-ray diffraction experiments

Diffraction experiments are a powerful approach claiming to yield unambiguous information about the local atomic structure in disordered materials.

Neutron diffraction measurements were performed in a relatively broad momentum transfer range, Q, combining the data measured by the 2-axis 'PSD' monochromatic neutron diffractometer (λ_0=1.068 Å; Q=0.45-9.8 Å^{-1}) [22] at the 10 MW Budapest research reactor and by the '7C2' diffractometer at the LLB-CEA-Saclay (λ_0=0.726 Å) [23]. The powder specimens of about 3-6 g/each were filled in thin walled cylindrical vanadium sample holder of 8 and 6 mm diameter for the two neutron experiments, respectively. Data were corrected for detector efficiency, background scattering and absorption effects. The structure factors, $S(Q)$s were evaluated from the raw experimental data, using the programme packages available at the two facilities. As far as, the statistics of the data is better for the PSD at low-Q values (below ~4 Å^{-1}), while the statistics of 7C2 data is better above 8 Å^{-1}, therefore the $S(Q)$ data were combined by normalizing the PSD data to the 7C2 in the 4-8 Å^{-1} interval by least square method. The agreement of the corresponding $S(Q)$ values was within 1% in the overlapping Q-range. The average values of the two spectra were used for further data treatment. For Q<4 Å^{-1} the PSD data, only, and for Q>8 Å^{-1} the 7C2 data were used. The $S(Q)$ data were obtained with a good signal-to-noise ratio up to Q_{max}=16 Å^{-1}. Diffraction experiments for high-Q values are necessary to obtain fine r-space resolution of the atomic distribution function analyses.

Figure 2a shows the ND experimental $S(Q)$ data for the investigated samples together with the results of RMC simulation (details of the RMC modelling will be discussed in the next section). The overall run of the ND experimental curves is very similar for the investigated samples, only slight differences may be observed, especially at low-Q values for the intensive first peak at 1.6 Å^{-1}. The next intensive peaks are at 3.05 Å^{-1} and at 5.5 Å^{-1} for all compositions. Oscillations were measured up to high-Q values, which is a fingerprint for well-defined short-range order.

X-ray diffraction studies were performed at the beam line BW5 at Hasylab, Desy [24]. The fine powdered samples were filled into special quartz capillary tubes of 2 mm in diameter (wall thickness of ~0.02 mm) and measured at room temperature. The energy of the radiation was 109.5 keV (λ_0=0.113 Å). The high-energy synchrotron X-ray radiation makes it possible to reach diffraction data up to high-Q values. In this study the XRD structure factors were obtained up to 20-22 Å^{-1}, for higher Q-values the experimental data proved to be noisy. Figure 2b shows the $S(Q)$ data obtained from XRD experiments for the investigated samples together with the results of RMC simulation. It is obvious, that the XRD spectra are very different from the ND ones. The main difference is that the first intensive peak is at 2.1 Å^{-1}, a small peak at 3.1 Å^{-1}, a broad peak at 5 Å^{-1} and at 8.6 Å^{-1}.
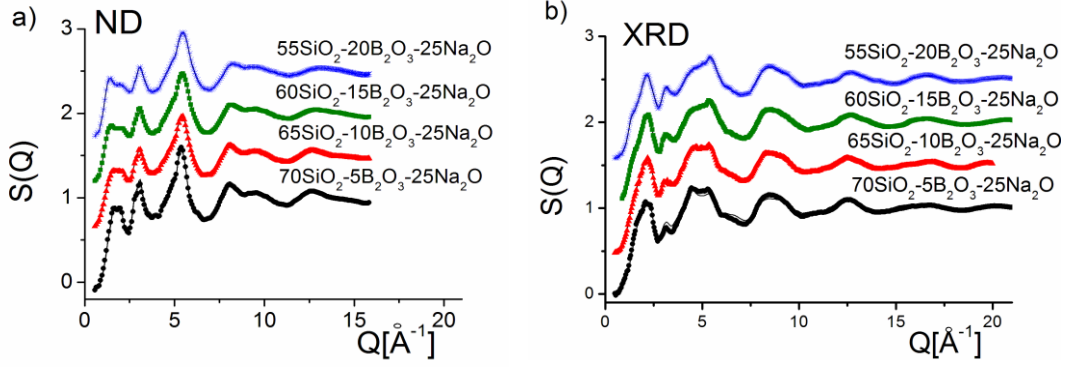
Figure 2. a) Neutron diffraction and **b)** X-ray diffraction total structure factors for (75-x)SiO$_2$-xB$_2$O$_3$-25Na$_2$O glasses: x=5 (black circle), x=10 (red triangle), x=15 (green square), x=10 (blue cross) glasses and RMC fits (solid line). (The curves are shifted vertically by 0.6 for clarity)

The differences in the overall run of the ND and XRD spectra are the consequence of the different values of the weighting factors, w_{ij}, of the partial structure factors, $S_{ij}(Q)$, defined as:

$$S(Q) = \sum_{i,j}^{k} w_{ij} S_{ij}(Q),$$ (1)

$$w_{ij}^{ND} = \frac{c_i c_j b_i b_j}{\left[\sum_{i,j}^{k} c_i b_j \right]^2},$$ (2)

$$w_{ij}^{XRD}(Q) = \frac{c_i c_j f_i(Q) f_j(Q)}{\left[\sum_{i,j}^{k} c_i f_i(Q) \right]^2},$$ (3)

where c_i, b_i and f_i are the molar fraction, coherent neutron scattering length and the atomic scattering factor for atoms of type i, respectively. The dependency of f_i on the scattering vector Q and the X-ray energy leads to a convolution in real space between the Fourier transforms of the weighting factors and partial pair correlation functions. The neutron scattering amplitude of an element is constant in the entire Q-range [25], while the X-ray scattering amplitude is Q-dependent [26]. Tables 1 and 2 shows the corresponding weighting factors, w_{ij} for the two radiations, w_{ij}^{ND} and $w_{ij}^{XRD}(Q)$ at Q=0.87 Å^{-1}.

Table 1. Neutron diffraction weighting factors of the partial interatomic correlations in sodium borosilicate glasses.

Atom pairs	ND weighting factor (%)			
	SiB5NaO	SiB10NaO	SiB15NaO	SiB20NaO
Si-O	22.09	18.63	15.56	13.46
B-O	8.02	13.77	18.94	22.53
O-O	42.30	40.59	39.10	38.10
Na-O	15.36	13.83	12.35	11.25
Si-Si	2.88	2.13	1.55	1.18
Si-Na	4.01	3.17	2.45	1.98
Si-B	2.09	3.16	3.77	3.98
B-B	0.38	1.16	2.29	3.33
B-Na	1.45	2.34	2.99	3.32
Na-Na	1.39	1.17	0.97	0.83

Table 2. X-ray diffraction weighting factors (at Q=0.87 Å^{-1}) of the partial interatomic correlations in sodium borosilicate glasses.

Atom pairs	XRD weighting factor (%)			
	SiB5NaO	SiB10NaO	SiB15NaO	SiB20NaO
Si-O	29.27	27.30	25.23	23.53
B-O	2.30	4.36	6.62	8.51
O-O	23.52	24.99	26.60	27.96
Na-O	18.39	18.34	18.10	17.79
Si-Si	9.10	7.46	5.98	4.95
Si-Na	11.44	10.02	8.58	7.49
Si-B	1.43	2.38	3.14	3.58
B-B	0.06	0.19	0.41	0.65
B-Na	0.90	1.60	2.25	2.71
Na-Na	3.59	3.36	3.08	2.83

It can be seen that for the Si-O weights we get significant values for both radiations. The weights of B-centred partials are more significant in neutron experiment. While the Na-O weights are higher in X-ray data than in neutron data. The O-O contribution has a dominant weight in the neutron experiment, in contrast to the X-ray case. Taking into consideration all these characteristics, we can conclude that the two radiations give complementary information and, both type of measurements are needed to obtain a real structure for the investigated samples.

3. Reverse Monte Carlo modelling and results

Reverse Monte Carlo (RMC) method was used to improve the analysis of the neutron and X-ray experimental spectra's [27]. RMC simulations are routinely used in to extract 3-dimensional atomic models in the literature quantitative agreement with the experimental data. The RMC algorithm represents a non-linear fit of the pair distribution function of a model structure to the experimental data, which unavoidably contain statistical and even in some cases leftover systematic errors. Therefore, the range of the possible structural models, created by the RMC simulation, will depend on the information content of the experimental data. During RMC process, the partial structure factors, $S_{ij}(Q)$ is calculated from the pair distribution functions $g_{ij}(r)$ via a Fourier transform,

$$S_{ij}(Q) = 1 + \frac{4\pi\rho_0}{Q} \int_0^{r_{max}} r\left[g_{ij}(r) - 1\right]\sin Qr\, dr, \qquad (4)$$

where r_{max} is the half edge-length of the simulation box of the RMC calculation. The actual computer configuration is modified by moving the atoms randomly until the calculated $S(Q)$ (see eqs.(1)-(3)) agrees with the experimental data within the experimental error. Moves are only accepted if they are in accordance with certain constraints (see below those ones which were applied in this work).

The parameters of the RMC calculations were as follows. For the starting configuration we used the results obtained for binary SiO_2-Na_2O [13] and B_2O_3-Na_2O [14] glasses. The simulation box contained 10,000 atoms with density 0.079, 0.078, 0.077 and 0.075 atoms·Å^{-3} and half-box length r_{max}=25.10, 25.21, 25.32 and 25.54 Å for the SiB5NaO, SiB10NaO, SiB15NaO and SiB20NaO glasses, respectively. Two types of constraints were used, the minimum interatomic (cut-off) distances and coordination constraints. We applied two types of constrains, a positive and a negative coordination constrains. The Si atoms were constrained to be coordinated by 4 O atoms as a positive constrain, and a negative constrains that not coordinated 1 and/or 2 O atoms. While B atoms were constrained to be not coordinated both by 1 and 2 O atoms. The RMC technique minimizes the squared difference between the experimental $S(Q)$ and the calculated one by moving the atoms randomly. In the present study both neutron and X-ray diffraction data were used simultaneously in the RMC calculations. The converged calculation gave an excellent fit of the experimental structure factors, as it is shown in Figure 2. The final set of the cut-off distances are tabulated in Table 3.

**Table 3.** Cut-off distances (Å) for atom pairs used in the final RMC run

Atom pairs	Cut-off distance (Å)			
	SiB5NaO	SiB10NaO	SiB15NaO	SiB20NaO
Si-O	1.55	1.55	1.55	1.55
B-O	1.2	1.3	1.3	1.3
Na-O	2.22	2.22	2.2	2.2
O-O	2.33	2.33	2.33	2.34
Si-Si	2.93	2.93	2.94	2.93
Si-Na	2.8	2.8	2.8	2.8
Si-B	2.6	2.6	2.6	2.6
Na-B	2.4	2.4	2.4	2.4
B-B	2.54	2.54	2.56	2.53
Na-Na	2.8	2.8	2.8	2.8

Information about the local atomic structure in glassy materials allows calculations of all the partial structure factors and partial pair distribution functions. The partial structure factors $S_{i\text{-}O}(Q)$ of glasses determined by applying the RMC simulation technique are displayed in Fig. 3.
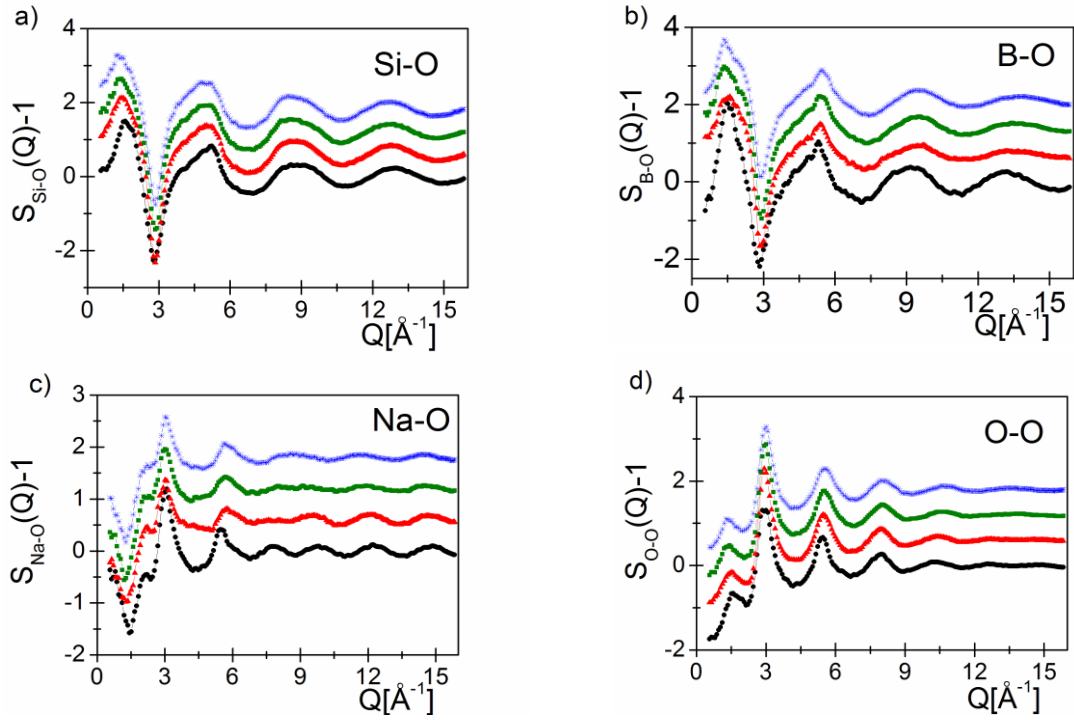
Figure 3: Partial structure factors for the SiB5NaO (black circle), SiB10NaO (red triangle), SiB15NaO (green square), SiB20NaO (blue crosses) glasses obtained by RMC modelling: a) Si-O; b) B-O; c) Na-O and d) O-O atom pairs.

The results for several partial atomic pair correlations, $g_{ij}(r)$ obtained from the RMC simulation are displayed in Fig. 4, while the interatomic distances are gathered in Table 4. The $g_{ij}(r)$ functions reflects the changes in the dependence of B_2O_3 concentration remarkably well.
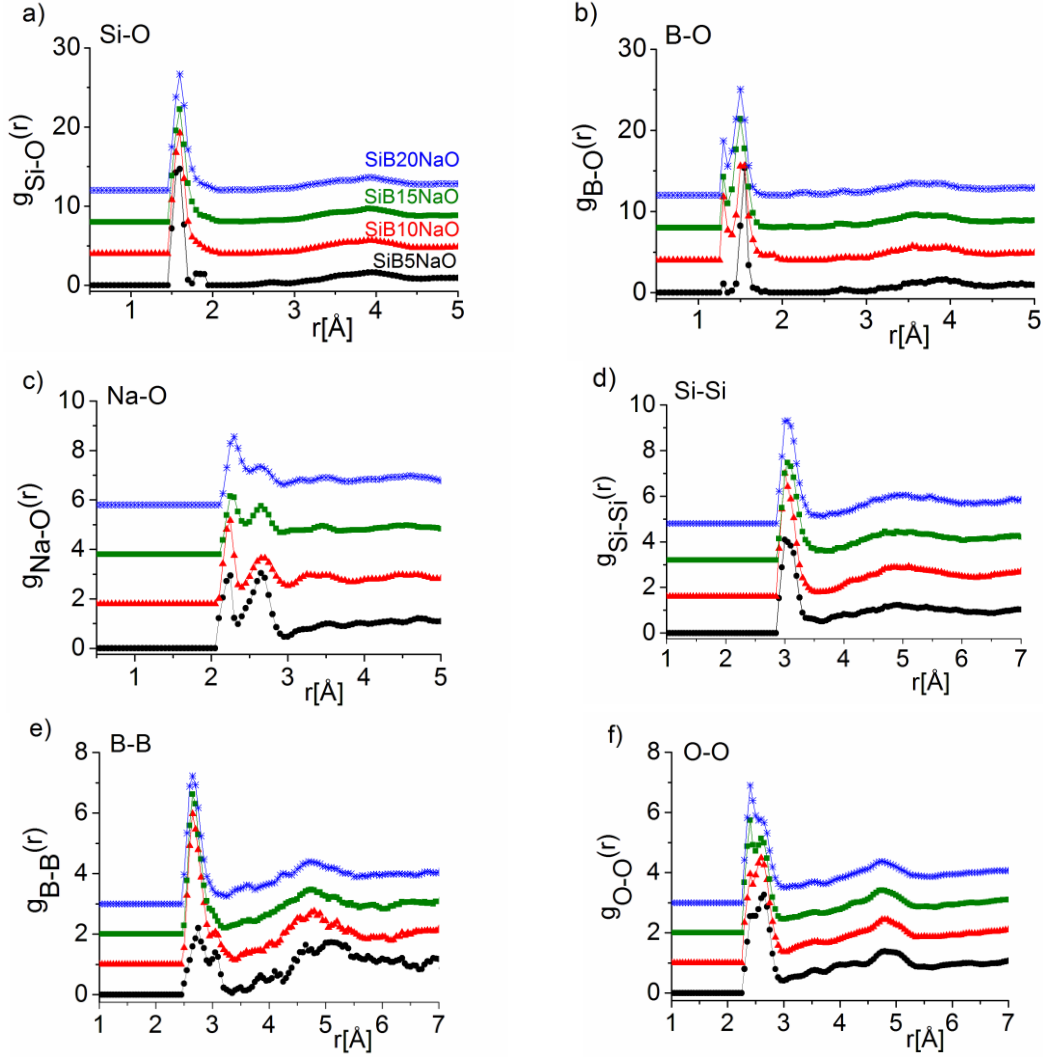
Figure 4: Partial atom pair correlation functions for the SiB5NaO (black circle), SiB10NaO (red triangle), SiB15NaO (green square), SiB20NaO (blue crosses) glasses obtained by RMC modelling: a) Si-O; b) B-O; c) Na-O; d) Si-Si, e) B-B and f) O-O atom pairs. The curves are shifted vertically by 1.0 and 1.9 for clarity.

Next we present our results for those atomic pair correlation functions, which have relatively high weighting factor.

Table 4. Interatomic distances, r_{ij} (Å) in sodium borosilicate glasses obtained from RMC simulation. The error bars are estimated from the reproducibility of various RMC runs.

| Atom pairs	Interatomic distances, r_{ij} (Å)			
	SiB5NaO	**SiB10NaO**	**SiB15NaO**	**SiB20NaO**
Si-O	1.60±0.01	1.60±0.01	1.60±0.01	1.60±0.01
B-O	1.30/1.55±0.05	1.30/1.55±0.05	1.30/1.50±0.05	1.30/1.50±0.05
Na-O	2.25/2.65±0.05	2.25/2.65±0.05	2.25/2.65±0.05	2.25/2.65±0.05
O-O	2.45/2.65±0.05	2.40/2.60±0.05	2.40/2.60±0.05	2.40/2.60±0.05
Si-Si	3.0±0.05	3.0±0.05	3.05±0.05	3.05±0.05
B-B	2.75±0.1	2.65±0.1	2.65±0.1	2.6±0.1

The first peak of $g_{Si-O}(r)$ is a narrow and symmetric one, centred at 1.60 Å, and for all investigated samples they are rather similar. Similarly, in to the $g_{Si-Si}(r)$ we obtained peak at position 3.0 (and 3.05) Å for all compositions. This means that the Si-O network is highly stable, and its main characteristic features don't change with the increasing amount of B_2O_3 content.

The first peak of $g_{B-O}(r)$ splits into two sub-peaks, with peak positions at 1.30 Å and 1.5(5) Å. The relative intensities of the sub-peaks depend on the boron concentration. With increasing B_2O_3 concentration the intensity of the first sub-peak increases, while the second peak decreases. The position of the sub-peaks is constant within limit of error. The $g_{B-B}(r)$ shows a characteristic distribution, with a first peak centred at 2.65 and 2.75 Å.

The $g_{Na-O}(r)$ pair correlation function shows a double peak at 2.25 Å and 2.65 Å. It can be seen that the sub-peak intensity changes with changing boron concentration, for the low boron containing sample, the peaks have the same intensity while the contribution of the sub-peak at higher Q-value slightly decreases as the B_2O_3 concentration is increased. This is so even that the concentration of Na_2O is the same for all samples.

The $g_{O-O}(r)$ pair correlation functions show very similar run for all samples. A broad distribution appears with two sub-peaks at 2.4 Å and 2.65 Å. The intensity ratio of the two peaks depends on the SiO_2/B_2O_3 content, the intensity of the first peak increases, while the second decreases with increasing boron content.

It is a great feature of the RMC method that the coordination number CN_{ij} can be obtained from the configurations. From the partial pair distribution functions we calculated the number of nearest neighbours for Si, B, Na and O atoms using the corresponding bond cut-off distances for Si-O, B-O, Na-O and O-O. It is necessary to specify a range in r over which atoms are counted as neighbours. This can be understanding of as defining coordination shells. Introducing r_1 and r_2, where r_1 and r_2 are the positions of minimum values on the lower and upper side of the corresponding peak. In Table 5, we present the average coordination numbers, and these results are summarized in Fig. 5.
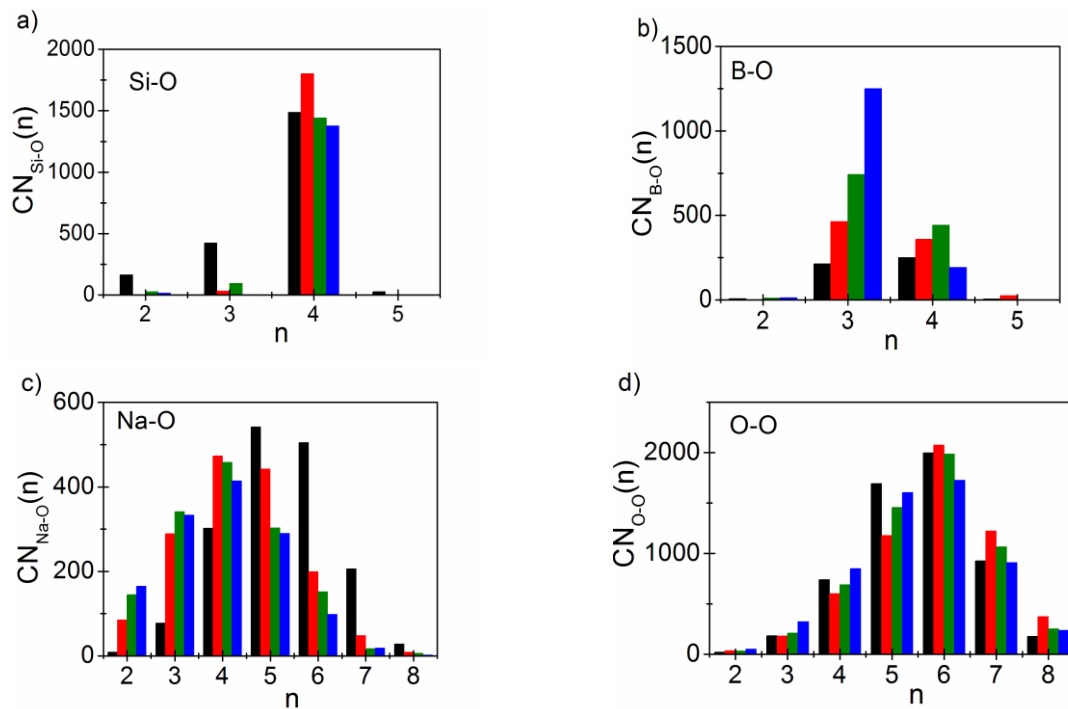
Figure 5. Coordination number distributions for SiB5NaO (black), SiB10NaO (red), SiB15NaO (green), SiB20NaO (blue) glasses from RMC modelling: a) Si-O; b) B-O; c) Na-O and d) O-O atom pairs.

Table 5. Average coordination numbers, CN_{ij} calculated from RMC simulation. In brackets the interval is indicated, where the actual coordination number was calculated. The error is ~5% for Si-O and B-O and ~10% for Na-O and O-O (except of SiB5NaO, where the error is ~10% for Si-O and B-O and ~10% for O-O). Relative abundance (in %) were calculated from RMC configuration.

Atom pairs	Coordination number, CN_{ij} (atom)			
	SiB5NaO	SiB10NaO	SiB15NaO	SiB20NaO
Si-O	3.6 (r_1:1.5-r_2:1.9)	3.95(r_1:1.5- r_2:1.95)	3.9 (r_1:1.5- r_2:1.8)	3.9 (r_1:1.5- r_2:2.0)
2-fold O coordination	8	0.5	2.6	2
3-fold O coordination	20.3	1.7	2.3	2.6
4-fold O coordination	**71.7**	**97.8**	**95.1**	**95.4**
B-O	3.45 (r_1:1.3- r_2:1.8)	3.5 (r_1:1.25- r_2:1.85)	3.35 (r_1:1.25- r_2:1.85)	3.1 (r_1:1.25- r_2:1.8)
2-fold O coordination	1.7	0.2	1.5	1.8
3-fold O coordination	**44.6**	**54.8**	**62.3**	**85.1**
4-fold O coordination	**52.7**	**42.1**	**36.2**	**13.1**
5-fold O coordination	1	2.9	-	-
Na-O	5.3 (r_1:2.15- r_2:2.85)	4.3 (r_1:2.15- r_2:2.9)	4.0 (r_1:2.15- r_2:2.85)	3.85 (r_1:2.15- r_2:2.85)
2-fold O coordination	0.5	6.6	11.9	14.8
3-fold O coordination	4.6	18.5	23.5	24.5
4-fold O coordination	18.1	30.3	31.8	30.5
5-fold O coordination	32.6	28.2	20.9	21.4
6-fold O coordination	30.2	12.7	10.4	7.2
7-fold O coordination	12.3	3.1	1.1	1.3
8-fold O coordination	1.7	0.6	0.4	0.3
O-O	5.55 (r_1:2.3- r_2:3.0)	5.85 (r_1:2.35- r_2:3.1)	5.65 (r_1:2.3- r_2:3.0)	5.5 (r_1:2.3- r_2:3.0)
2-fold O coordination	0.3	0.6	0.5	0.9
3-fold O coordination	3.2	3.1	3.7	5.6
4-fold O coordination	12.9	10.4	12.2	14.9
5-fold O coordination	29.5	20.6	25.4	27.4
6-fold O coordination	34.7	36.1	34.5	30.5
7-fold O coordination	16.1	22.3	18.5	15.9
8-fold O coordination	3.3	7.8	5.2	4.8

It can be seen that the average oxygen coordination number around Si atoms is very close to 4 atoms, as proposed by the formation of tetrahedral units in the network, however, with increasing boron content the Si-O coordination number, CN_{Si-O} slightly decreases from 3.95 to 3.9 atoms (except of SiB5NaO) indicating a little bit distorted but close of ideal tetrahedral surrounding. This may be caused by the formation of mixed Si-O-B chains, where boron atoms are coordinated by both 3 and 4 oxygen atoms (see Fig. 5/b). The average CN_{B-O} coordination number decreases from 3.5 to 3.1 (except of SiB5NaO) with increasing boron content. This suggests that the glassy network consists of trigonal and tetrahedral boron units. The Na-O coordination number continuously decreases with increasing B_2O_3 concentration, from 5.3 to 3.85. The O-O average coordination number is ~5.6 atoms, and slightly decreases with increasing boron concentration.

We have calculated the three-particle bond-angle distributions using the final atomic configuration of the RMC algorithm, plotted both as the function of $cos(\Theta)$ (scale below) and Θ (upper scale), where Θ represents the actual bond angle. Figure 6 shows the distributions for the network former atoms: Si-O-Si, O-Si-O, B-O-Si, B-O-B, O-B-O and O-O-O.
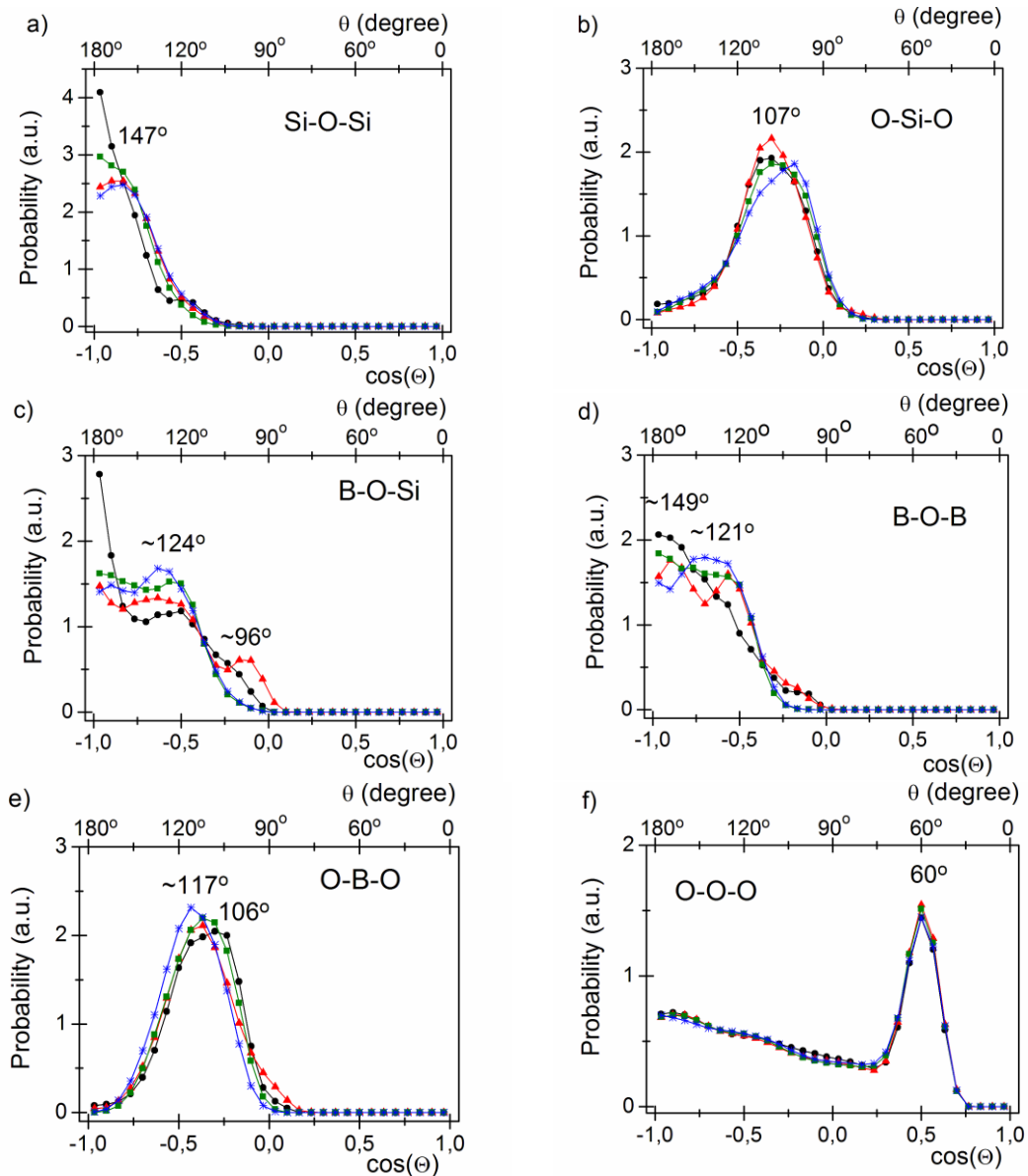
Figure 6. Three-particle bond-angle distributions obtained from RMC simulation for SiB5NaO (black circle), SiB10NaO (red triangle), SiB15NaO (green square), SiB20NaO (blue cross): a) Si-O-Si; b) O-Si-O; c) B-O-Si; d) B-O-B; e) O-B-O; f) O-O-O.

For the Si-O-Si and O-Si-O the peak positions are at 147±3° and 107±5°, respectively, which are very close values to the ideal tetrahedral configuration. Vitreous B_2O_3 forms glass which contains only BO_3 networks made up from boroxol groups and BO_3 triangles. The addition of a modifier initially converts BO_3 triangles into BO_4 tetrahedra, increasing coordination number and strengthens the network. A boron atom with coordination number 4 in the network allows the possibility to establish a different kind of superstructural units to the boroxol group. This superstructural unit contains BO_4, beside BO_3 as it is typical found in glasses. The broad distribution of B-O-B bonding angles are quite asymmetric show distribution, the average angles being 121±5° and 149±5°. This broad distribution suggest that both 3-fold B atoms and 4-fold B atom are present. This is a sign of possible formation of new superstructural units. The O-B-O bond angles distribution shows a peak at 106±5°, similarly characteristic and close to the O-Si-O distribution, however, a shifting can be observed with the increase of boron concentration up to the 117±5°, implying considerable distortion in BO_3 planar geometry. The B-O-Si distribution show a peak at 96±7° at lower boron concentration, this disappear at SiB15NaO and SiB20NaO samples, and they shows a characteristic distribution at 124±7°. The O-O-O bond angle distribution show peaks centred at 60±1°, as it is illustrated in Fig.6/f.

4. Discussion

The network structure of binary SiO_2-Na_2O [13 and references therein] and B_2O_3-Na_2O [14 and therein] glasses is very different, therefore the structural characterization of the ternary SiO_2-B_2O_3-Na_2O glass is a big challenge. We performed RMC modeling on neutron and X-ray data. The partial and total structure factors together with the experimental data and the partial-pair correlation functions, coordination number distributions and three particle bond angle distributions were obtained. Figures 3 and 4 compares the partial structure factors and the partial pair correlation functions for the four glasses. Obviously, the main features are very similar to each other, however, the concentration dependence may be observed.

In our present study, we were found that the Si atoms are 4-fold oxygen coordinated forming SiO_4 tetrahedral units, similarly to the basic network structure of binary SiO_2-Na_2O glass [13]. The Si-O distribution shows characteristic peak at 1.60 Å for all four samples (see Fig. 4/a and Table 4), which is slightly shorter than the first neighbour distance at 1.615 Å in v-SiO_2 [28], or 1.62 Å in SiO_2-Na_2O [13], however, agrees well with the distance 1.60 Å obtained for the multi-component sodium borosilicate glasses [15]. The tetrahedral Si environment is substantiated by the straight Si-O-Si bond angle at 147° and the O-Si-O with a stable 107° peak for all four samples, similarly as in almost all silicate materials [29, 30, 31].

The neighbourhood of boron atoms proved to be rather complex. We have revealed both 3-fold (BO_3) and 4-fold (BO_4) oxygen coordination (see Fig. 5/b) from RMC modelling, and two distinct first neighbour distance at 1.30 Å and 1.5(5) Å (see Table 4). The relative abundance of BO_3 and BO_4 units compared to the total number of B-O neighbours depend on the B_2O_3 content. With increasing boron content the fraction of 4-coordinated boron decreases with simultaneously increasing of 3-coordinated fraction. Finally, for the sample with x=20 mol% most of the boron atoms, 85% are 3-fold coordinated. These results are in agreement with NMR investigations, as well [20, 32]. With increasing B_2O_3 content (x=5, 10, 15 and 20 mol%) the number of BO_4 units decreases (52.7, 42.1, 36.2 and 13.1 %), while the number of BO_3 increases (44.6, 54.8, 62.3 and 85.1 %), and consequently the average CN_{B-O} decreases, i.e. 3.4, 3.5, 3.35 and 3.1 atoms, respectively. With increasing boron content, -parallel with the increasing of the number of BO_3 units-, the intensity of the $g_{B-O}(r)$ correlation function centred at 1.30 Å also increases. Consequently, the first neighbour distance at 1.30 Å can mainly be attributed to the 3-fold oxygen coordinated boron atoms, however, the 4-fold oxygen coordinated boron atoms also contribute to the formation of this $g_{B-O}(r)$ first sub-peak as well, in fairly good agreement with the result obtained from model calculations for a similar composition 55.3SiO_2-14.71B_2O_3-29.99Na_2O (d_{B-O}=1.44 Å) in ref. [33] and binary samples Na_2O-B_2O_3 [34] see Table 4. Regarding the B environment, the first asymmetrical peak suggests that well-defined BO_3 and BO_4 units are present in the glass structure, whereas the second symmetrical peak suggests the presence of the intermediate units between BO_3 and BO_4 [35]. At high boron concentration we find that the O-B-O angle is distributed around 117° near 120°, which indicates a distorted BO_3 planar geometry, in fairly good agreement with MD simulation results obtained for boron trioxide [36, 34]. Based on the above, the following conclusions can be drawn: i) the Si-O and B-O correlations are close to each other, ii) the Si-O (close to 4) and B-O (3 and 4) coordination number overlap with each other, iii) the bond angle distribution connected to B and Si distribution correlates with the characteristic trigonal and tetrahedral unit formations. This together here indicates that the [4]Si-O-[4]B and [4]Si-O-[3]B mixed linkages are formed, similarly, as we have found for multi-component sodium borosilicate glasses loaded with BaO and ZrO [15].

Based on our previous works [14,15] and the results presented here we can conclude that these alkaline borosilicate glasses contain relatively regular triangle BO_3 and tetrahedral BO_4 units. The presence of such regular SiO_4, BO_3 and BO_4 units implies a similarity between the short-range structures in these glasses.

Na_2O act as a network modifier, promote the conversation of some BO_3 units to BO_4 units. Unfortunately $g_{Na-O}(r)$ and $g_{O-O}(r)$ overlap with each other, thus, the results have to be handled with care. The sodium coordination number for the simulated glasses decreases with x (Table 6). The relatively high coordination number and atomic distances connected to Na-O are in agreement with results obtained for similar compositions of Na-B-X-O structures [37,38]. Sodium atoms are network modifiers only and do not form real bond to other atoms in the glass network mixed linkages.

6. Conclusions

Neutron- and high-energy synchrotron X-ray diffraction experiments were performed on the $(75-x)SiO_2-xB_2O_3-25Na_2O$ x=5, 10, 15 and 20 mol% glasses. The structure factor has been measured over a broad momentum transfer range, between 0.4-22 Å^{-1}, which made fine *r*-space resolution possible for real space analysis. For data analyses and modeling the Fourier transformation and the RMC simulation techniques were applied. The partial atomic pair correlation functions, the nearest neighbour distances, coordination number distributions and average coordination number values and three-particle bond angle distributions have been revealed. The Si-O network proved to be highly stable consisting of SiO_4 tetrahedral units with characteristic distances at r_{Si-O}=1.60 Å and r_{Si-Si}=3.0(5) Å independently from the SiO_2/B_2O_3 content with constant Na_2O content. The behaviour of network forming boron atoms proved to be more complex. The first neighbour B-O distances show two distinct values at 1.3 Å and 1.5(5) Å and, both trigonal BO_3 and tetrahedral BO_4 units are present. The relative abundance of BO_4 and BO_3 units depend on the boron content, in such a way that with increasing boron content the number of BO_4 is decreasing, while BO_3 is increasing. From the analyses of the obtained structural parameters we have concluded that the glassy network is formed by trigonal BO_3 and tetrahedral BO_4, SiO_4 groups, forming mixed [4]Si-O-[3],[4]B bond-linkages. Na_2O proved to be a network modifier as it is often reported in the literature for similar systems.

These results help to understand the basic network structure of the newly prepared and studied SiO_2-B_2O_3-Na_2O-BaO-ZrO_2-UO_3-CeO_2-Nd_2O_3 glasses.

References
[1] Chun K. S., Kim S. S., Kang C.H. 2001 Journal of Nuclear Materials 298 150
[2] Yim M.S., Murtv K.L. JOM 2000 52 26
[3] Jantzen C.M., Brown K.G., Pickett J.B. 2000 WSRC-MS-2000-00307
[4] Wicks G.W. Savannah River Technology Center Report 1999 WSRC-MS-99-000082
[5] Stefanovsky S. V., Shiryaev A. A., Zubavitchus J. V., Veligjanin A. A., Marra J. C. 2009 Glass Phys and Chemistry 35 141
[6] Mishra R. K., Sudarsan V., Kaushik C. P., Raj K., Kulshreshtha S. K., Tyagi A. K. 2006 Journal of Nuclear Materials 359 132
[7] Liu G. K., Zhuang H. Z., Williams J. V., Vikhnin V. S. 2002 Physics of the Solid State 44 1433
[8] Shaozhan X., QinganM. 1986 Journal of Non-Crystalline Solids 80 195
[9] Roderick J. M., Holland D., Howes A. P., Scales C. R. 2001 Journal of Non-Crystalline Solids 293-295 746
[10] Lee S. K., Mibe K., Fei Y., Cody G. D., Mysen B. O. 2005 Physical Review Letters 94 165507
[11] Li H., Su Z., Li L., Strachan D. M. 2001 Journal of Non-Crystalline Solids 292 167
[12] Maniu D., Iliescu T., Ardelean I., Cinta-Pinzaru S., Tarcea N., Kiefer W. 2003 Journal of Molecular Structure 651-653 485
[13] Fabian M., Jovari P., Svab E., Meszaros Gy., Proffen T., Veress E. 2007 Journal of Physics: Condensed Matter 19 335209
[14] Fabian M., Svab E., Proffen T., Veress E. 2010 Journal of Non-Crystalline Solids 356 441
[15] Fabian M., Svab E., Proffen T., Veress E. 2008 Journal of Non-Crystalline Solids 354 3299
[16] Varga Zs., Surányi G., Vajda N., Stefánka Zs. 2007 Microchemical Journal 85 39
[17] Molnár G.L. Handbook of Prompt Gamma Activation Analysis with Neutron Beams Kluwer Academic Publishers, Dordrecht / Boston / New York 2004
[18] Révay Zs., Belgya T., Molnár G. L. 2005 Journal of Radioanalitical Nuclear Chemistry 265 261
[19] Slovenian NMR Centre, http://www.nmr.ki.si/600_magnet.html
[20] Lee S. K., Mibe K., Fei Y., Cody G. D., Mysen B. J.2005 Physical Review Letters 94 165507
[21] Lin-Shu D., Stebbins J. F. 2003 Journal of Non-Crystalline Solids 315 239

[22] Sváb E., Mészáros Gy., Deák F. 1996 Materials Science Forum 228 247; http://www.bnc.hu/
[23] Ambroise J. P., Bellissent R. 1984 Rev. Phys. Appl. 19 731; http://www-llb.cea.fr/en/
[24] Poulsen H., Neuefeind J., Neumann H. B., Schneider J. R., Zeidler M. D. 1995 Journal of Non-Crystalline Solids 188 63
[25] Hannon A. C. ISIS Disordered Materials Database 2006, http://www.isis.rl.ac.uk/disordered.
[26] Waasmaier D., Kirfel A. 1995 Acta Crystallographica A 51 416
[27] McGreevy R. L., Pusztai 1988 Molecular Simulations 1 359
[28] Floriano M. A., Venezia A. M., Defanello G., Svensson E. C., Root J. H. 1994 Journal of Applied Crystalline 27 271
[29] Petkov V., Billinge S. J. L., Shastri S., Himmel B. 2000 Physical Review Letters 85 3436
[30] Ispas S., Benoit M., Jund P., Jullien R. 2001 Physical Review B 64 214206
[31] Bouty O., Delaye J. M., Beuneu B., Charpentier T. 2014 Journal of Non-Crystalline Solids 401 27
[32] Du W. F., Kuraoka K., Akai T., Yazawa T. 2000 Journal of Materials Science 35 4865
[33] Kieu L. H., Delaye J. M., Cormier L., Stolz C. 2011 Journal of Non-Crystalline Solids 357 3333
[34] Umesaki N., Kita Y., Kirihara T., Iida T., Fukunaga T., Misawa M. 1994 Journal of Non-Crystalline Solids 177 200
[35] Maths K., Michael S., Randilynn C., Philipp M., Steve W.M., Silvia I., Aleksandar M. 2015 Journal of Physical Chemistry C 119 (49) 27275
[36] Amini M., Mitra S. K., Hockney R. W. 1981 Journal of Physics C: Solid State Physics 14 3689
[37] Chen X., Li M., Chang X., Zang H., Xiao W. 2007 Journal of Solid State Chemistry 180 1658
[38] Wu L., Zhang Y., Chen X. L., Kong Y. F., Sun T. Q., Xu J. J., Xu Y. P. 2007 Journal of Solid State Chemistry 180 1470